Title: Evidence of Matuyama-Brunhes transition in the cave sediment in Central Europe

Hakan Ucar[1*], Gunther Kletetschka[1,2,3], Jaroslav Kadlec[4]

[1]Faculty of Science, Charles University, Prague, Czech Republic, [2]The Czech Academy of Sciences, Institute of Geology, Czech Republic, [3]Geophysical Institute, University of Alaska Fairbanks, AK, USA, [4]Institute of Geophysics, Czech Academy of Sciences, Czech Republic.

Abbreviated title: Matuyama-Brunhes record from the European cave sediment

*Corresponding author: Hakan Ucar; ucarh@natur.cuni.cz

Co-author's emails: gunther.kletetschka@natur.cuni.cz; kadlec@ig.cas.cz

Summary

In this study, we identified the Matuyama-Brunhes magnetic reversal recorded in cave sediments in Central Europe, Czech Republic. We collected discrete samples from the homogeneous sedimentary profile in the Za Hajovnou cave located in the eastern part of the Czech Republic. Novel use of characteristic remanent magnetization (ChRM) directions and VGP (Virtual Geomagnetic Pole) path of the data revealed the Matuyama-Brunhes transition boundary within 5.7 cm of the Za Hajovnou cave sediment. This result revealed a new more detailed behavior of the polarity transition from the central European location. The migration of the paleopole between east of Africa and west of North America is a significant marker for the central European paleomagnetic record in terms of global magnetic data. The precursor of the reversal occurs 4.6 kyr before the transition. As a result of the rock magnetism measurements, the magnetic carrier of the samples is maghemite. Also, we estimated the sedimentation rate of the cave for the first time.

Keywords: Paleomagnetism; Matuyama-Brunhes, magnetic reversal; cave; sediments

1. Introduction

Matuyama-Brunhes magnetic reversal occurred approximately 781 kyr ago (Gradstein et al. 2004). Published studies (Channel et al., 2010; Sagnotti et al., 2010, 2014; Suganuma et al., 2010; Jin and Liu, 2011; Giaccio et al., 2013; Kitaba et al., 2013; Pares et al., 2013; Valet et al., 2014; Liu et al., 2016; Okada et al., 2017; Bella et al., 2019) showed that this event is well recorded by respective sediments that had sufficient sedimentation rate and could be analyzed, in detail, by paleomagnetism. Also, studies in the recent years have shown a younger age for the reversal around 773 kyr (Channell et al., 2010 (773 ± 0.4 kyr); Suganuma et al., 2015 (770.2 ± 7.3 kyr); Simon et al., 2019 (773.9 kyr); Singer et al., 2019 (773 ± 2 kyr); Valet et al., 2019 (772.4 ± 6.6 kyr); Haneda et al., 2020 (772.9 ± 5.4 kyr)).

Sediments acquire remanent magnetization during their deposition. The alignment of magnetic moments of the grains occurs in the direction of the earth's magnetic field and acquisition of primary magnetization due to this sedimentation process is called depositional or detrital remanent magnetization (DRM) (Gubbins and Herrero, 2017). Remanent magnetization protected by potential energy barriers can last over geologic time scales. Nevertheless, due to thermal and/or chemical processes such as reheating, oxidation and formation of iron hydroxides during the time, secondary magnetizations can be acquired by crossing potential energy barriers or generation of chemical remanences. The new secondary magnetization has an orientation in the direction of the Earth's field. Then rocks can acquire a viscous remanent magnetization (VRM) a long time after their formation due to exposure to the geomagnetic field. VRM contributes to noise in paleomagnetic data (Butler, 1992; Lanza and Meloni, 2006).

Lock-in-depth affects the nature of the paleomagnetic recording process in sediments. It is defined as the depth at which the remanent magnetization is stabilized. Lithology, grain-size distribution of the sediment matrix, sedimentation rate and bioturbation, all have an influence on the position of the lock-in-depth in the sediments (Bleil and von Dobeneck, 1999; Sagnotti et al., 2005). When assuming the steady sedimentation rate, the result of lock-in-depth stabilization is younger magnetization than the sediment itself by an amount of time required to accumulate a sediment layer of thickness that equal to the lock-in-depth. For example, if the sediment has an accumulation speed of 1 mm per 1000 years, and lock-in-depth is 10 mm, the magnetization age is 10 000 years younger than the sediment itself (Sagnotti et al., 2005). Kadlec et al. (2005, 2014) reported that the Central European cave (local name "Za Hajovnou") in the Moravia region of the Czech Republic records the Matuyama-Brunhes transition. The aim of our study is to analyze the reversal in detail paleomagnetic method and to identify the magnetic carrier of the cave sediment. Here, we obtained a new paleomagnetic dataset from three vertical sediment profiles found in this cave. A central European paleomagnetic record of the B/M boundary will be valuable for investigation of the characteristic behavior of the Earth's magnetic field during Matuyama-Brunhes magnetic reversal. The sedimentation rate of the cave sediment is not known yet in terms of understanding the transition. It makes our estimation even more crucial in this study.

1.1 Geology of the Cave

The Za Hájovnou Cave (49° 40′ N, 16° 55′E) is a former sinkhole located in Javoricko Karst, Moravia Region of the Czech Republic (Lundberg et al., 2014; Musil, 2014) (Fig. 1). The Javoricko Karst is formed by light-grey-colored massive Devonian limestone that overlies Pre-Cambrian phyllite (Lundberg et al., 2014; Musil, 2014). Spranek and Javoricka are two rivers that flow through the Jarovicko karst. While Za Hájovnou Cave is situated on the north-western bank of the Javoříčka river on the southern slope of a Pani Hora hill (Lundberg et al., 2014; Žák et al., 2018), both Spranek and Javoricka watershed may have contributed to the sediment development in this cave (Fig. 1).

The Za Hajovnou cave is approximately 500 m long system (Musil, 2005; Bábek et al., 2015). The cave's corridors were explored previously in a total length of ~200 m (Musil, 2014) (Fig. 2). The cave currently consists of two main parallel corridors with a slightly different sedimentological record (Musil et al., 2014); the first corridor (local name is "Excavated Corridor" which is used to be sinkhole entrance) and the other corridor (local name is "Birthday Corridor") has a separate entrance. These two corridors are connected by the Connecting Passage Corridor (Fig. 2). Sediments from the Excavated Corridor continue to Birthday Corridor and partially filled the Connecting Passage Corridor (Musil et al., 2014) (Fig. 2).

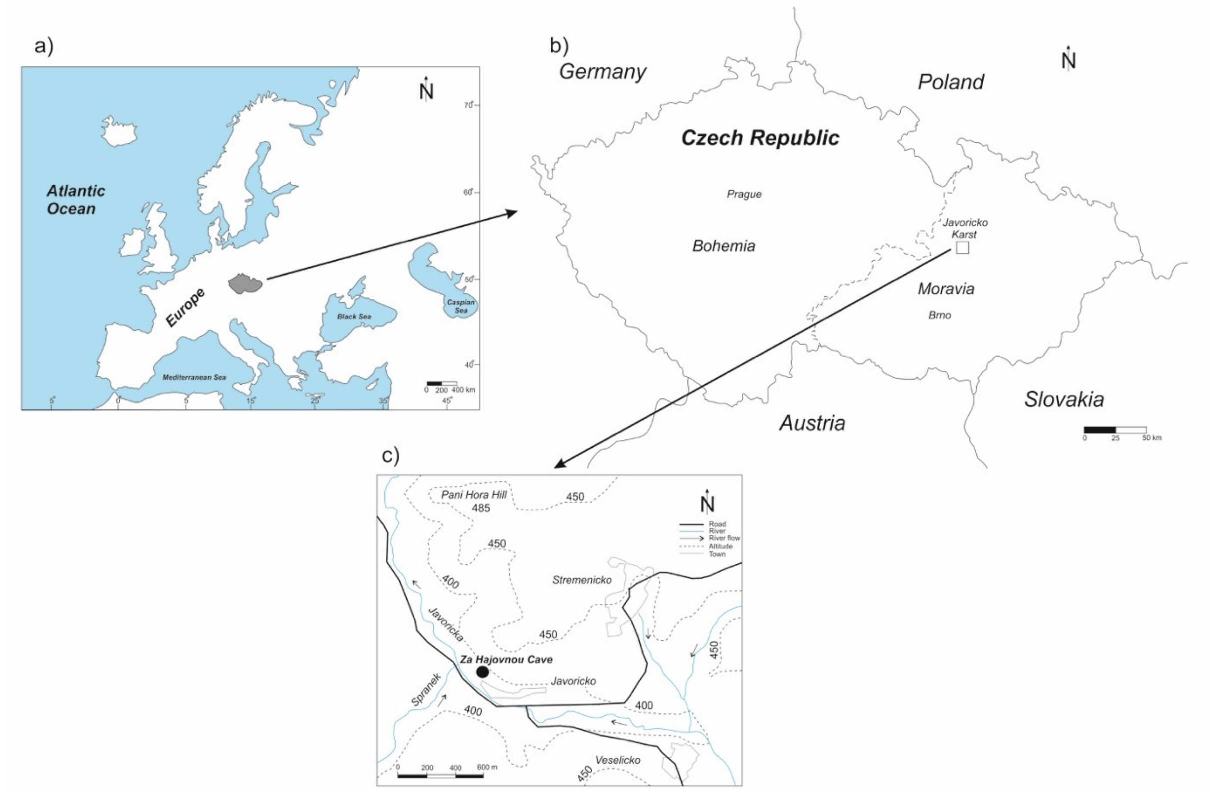

Fig. 1. Location of the study area in (a) Central Europe. Dashed lines in (b) show more detailed placement with different regions of the Czech Republic in relation to the study area. Map in (c) shows regional detail of the Za Hajovnou cave placement (modified after Lundberg et al., 2014; Musil, 2014).

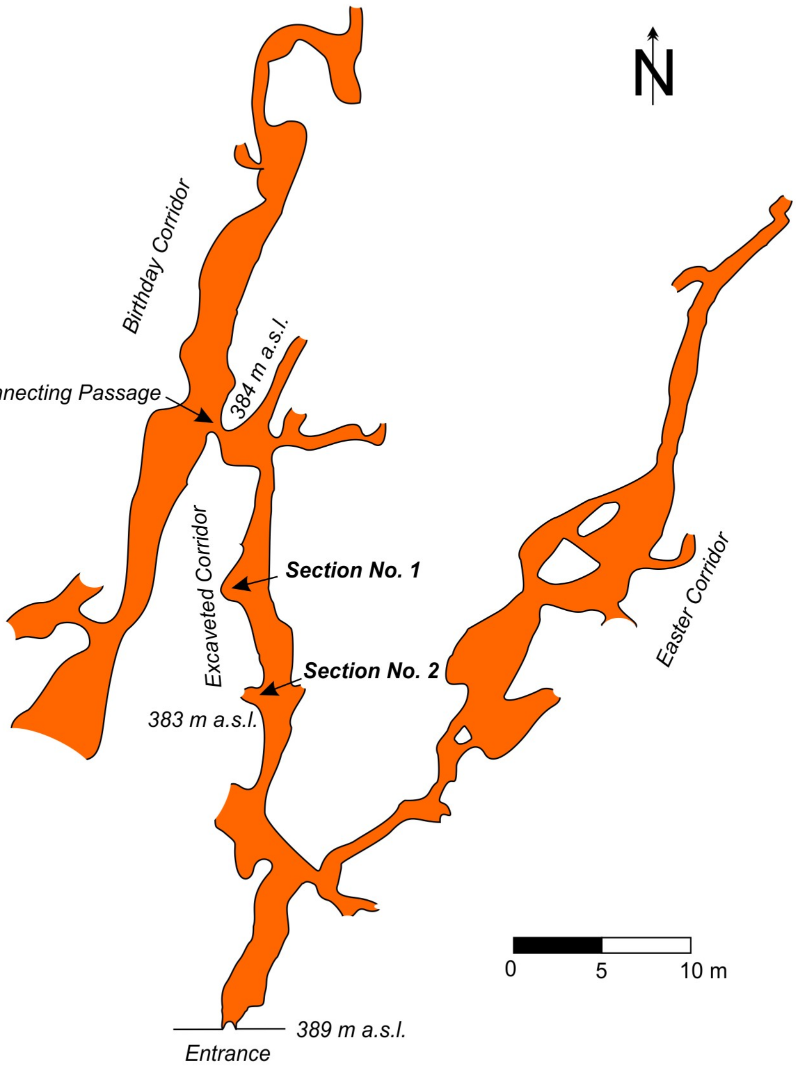

Fig. 2. Map of the Za Hajovnou cave (modified after Kadlec et al., 2014; Lundberg et al., 2014; Musil, 2014). Locations marked by "Section No. 1" and "Section No. 2" are discussed in the text (Kadlec et al., 2005, 2014). The map shows the relation between Connecting Passage Corridor, Birthday Corridor, and Excavated Corridor (m a.s.l.: meter above sea level).

Upper sediments of the cave were dated by U/Th dating of flowstones from 118 ± 1 to 267 ± 3 ka and the sediment sequence below was inferred to contain the Matuyama-Brunhes boundary in Section No. 1 (Fig. 3) (Musil, 2005; Kadlec et al., 2005, 2014; Lundberg et al., 2014; Bábek et al., 2015). The sedimentation in the cave corridors was active from the Early

Pleistocene until the beginning of the Middle Pleistocene. The sediment then consists of Pleistocene glacial time in north-western Europe called the Cromerian Interglacials complex (Muller, 1992), MIS19 (marine isotope stage) which is interglacial period ~780 ka (Pol et *al*., 2019), and Matuyama-Brunhes reversal (Kadlec et al., 2005, 2014; Lundberg et al., 2014; Musil, 2014; Musil et al., 2014; Žák et al., 2018).

The Matuyama-Brunhes boundary (781 ka) was suggested in the upper part of the backwater fine sediments, deposited from suspension in the flooded cave. These sediments underlay mostly non-fluvial deposits which entered the cave through a steep passage and filled the Connecting Passage Corridor (Kadlec et al., 2014; Lundberg et al., 2014; Musil et al., 2014). The total thickness of the sediments, deposited from suspension, reaches up to 4.3 m.

Sedimentary sections retrieved in the Za Hajovnou cave by Kadlec et al. (2005, 2014) were composed of two parts. The first part (Section No. 1, in Fig. 2) was situated in the Excavated Corridor about 28 m from the cave entrance (Kadlec et al., 2005) (Fig. 2). It was intepreted to contain the magnetic transition from a reversed to normal polarity and inferred from the age dates of the overlying non- fluvial sediments, that our data indicate that the reversal is the actual Matuyama-Brunhes reversal. Sediment thickness in the Section No. 1 is 0.8 m. The second sedimentary section (Section No. 2) partially overlapped the Section No. 1 and was located in the Excavated Corridor (Kadlec et al., 2014) (Fig. 2). Kadlec et al. (2014) indicated that this section had sediment with just reversed polarity except for the upper part of the sediment where the magnetization was difficult to interpret because the sediments had weak magnetization for which the sensitivity of the Agico JR-5A spinner magnetometer was insufficient. Section No. 2 underlies the Section No. 1 and contains older backwater sediment with reversed magnetic polarity (age > 781 ka) (Kadlec et al., 2014).

The difficulties in the interpretation of the primary study by Kadlec et al. (2014) was the motivation for the presented research. Here we collected 44 oriented discrete sedimentary samples from the Excavated Corridor near the upper backwater sedimentary Section No. 1 (Fig. 2, 3).

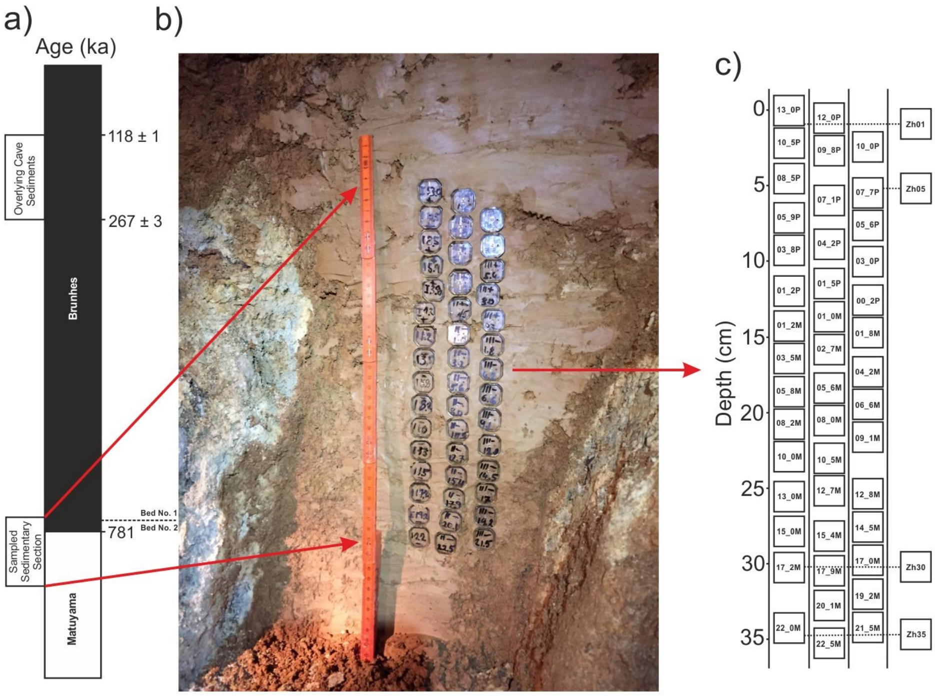

Fig. 3. Za Hajovnou cave sediments. (a) Age diagram of Za Hajovnou cave (dashed lines show the boundary between Bed No. 1 and 2), (b) sampled sedimentary Section No. 1, and (c) discrete samples for the paleomagnetism measurements and the rock magnetism samples (numbers show the sample name).

2. Materials and Methods

2.1. Preperation of the Samples

The sediment outcrop in the cave was made into a smooth plane and the samples for the paleomagnetism measurements were taken by pushing the plastic boxes (2x2x2 cm; 8cc) into the sediment (Fig. 3). We used a common geological compass (produced by the Brunton) for measuring the azimuth and tilt of the sample boxes. After the paleomagnetism sampling, another 4 samples were placed in the plastic boxes for the rock magnetism measurements (Fig. 3c). These samples were taken from the same depth as the paleomagnetic samples

(13_0P, 7_7P, 17_2M, 22_0M). The thickness of the sampled part of the sedimentary section was 35.1 cm. The upper backwater (water accumulation) fine sediment part was brown clayey silt with white angular clasts of weathered limestone and bone fragments (Bed No. 1) (Kadlec et al., 2014). The lower part of the section consisted of the brown silty clay without white clasts (Bed No. 2) (Kadlec et al., 2014) which is presented in Fig. 3.

2.2. Demagnetization Measurements

To clean the secondary magnetizations from the sedimentary samples, we applied a stepwise alternative field (AF) demagnetization method in Pruhonice Paleomagnetism Laboratory of Czech Academy of Sciences. This method was carried out using a 2G Enterprises Cryogenic Magnetometer on 44 samples divided into 3 different sequences. The first sequence was 17 samples (13_0P, 10_5P, 09_8P, 08_5P, 05_9P, 03_8P, 01_2P, 01_2M, 03_5M, 05_8M, 08_2M, 10_0M, 13_0M, 15_0M, 17_2M, 19_2M, 22_0M) where we demagnetized at 1 mT intervals between 0-49 mT and 10 mT intervals between 50-100 mT. The second sequence was 14 samples (12_0P, 07_1P, 04_2P, 01_5P, 01_0M, 02_7M, 05_6M, 08_0M, 10_5M, 12_7M, 15_4M, 17_9M, 20_1M, 22_5M) where we demagnetized at 2 mT intervals between 0-48 mT and 10 mT intervals between 50-100 mT. The third sequence was 13 samples (10_0P, 07_7M, 05_6P, 03_0P, 00_2P, 01_8M, 04_2M, 06_2M, 09_1M, 12_8M, 14_5M, 17_0M, 21_5M) and we demagnetized at 0.5 mT intervals between 0-39.5 mT and 10 mT intervals between 40-100 mT. Demagnetization data was interpreted by using Remasoft software which was written by Agico Company (Martin Chadima and Frantisek Hrouda).
Characteristic remanent magnetization (ChRM) directions and maximum angular deviation (MAD) values were determined from principal component analysis (PCA) (Kirschvink, 1980) on the Zijderveld diagram (Zijderveld, 1967). Virtual geomagnetic pole's (VGP's) latitudes and longitudes were calculated using PMGSC software by Randy Enkin. Table 1 shows the

data of alternative field demagnetization for each sample. Examples of alternative field demagnetization results for the Matuyama and Brunhes intervals (two examples each) are shown in Fig. 4. The rest of the samples are in the Supporting Information Tables S1 and Supporting Information Figs S2. Maximum angular deviation (MAD) values of this study and other studies (Sagnotti et al., 2014; Okada et al., 2017) are shown in Fig. 5.

Table 1. Alternative field demagnetization, virtual geomagnetic pole (VGP) data, and Matuyama-Brunhes magnetic reversal scale for this study. Minus (-) values for virtual geomagnetic pole (VGP) latitudes and longitudes indicate the southern and western hemispheres. MAD: maximum angular deviation, φ_p: VGP latitude, λ_p: VGP longitude.

Sample Name	Depth (cm)	Dec $^{(o)}$	Inc $^{(o)}$	Intensity (A/m)	MAD $^{(o)}$	φ_p (N°/S°)	λ_p (E°/W°)	
13_0P	0	369.2	65.9	7.56E-04	0.4	83.8	114.5	Brun

12_0P	-1	356.1	58.5	1.06E-03	1.8	79.4	-146.7	hes
10.5P	-2.5	379.7	37.8	8.03E-04	1.4	57.8	160.5	
10_0P	-3	407.1	44.3	7.96E-04	1.2	47	121.8	
09_8P	-3.2	401.1	33	1.04E-03	1	44.5	135.4	
08_5P	-4.5	378.5	43.2	7.02E-04	1.6	61.8	159.2	
07_7P	-5.3	378.7	25.2	7.47E-04	1.4	50.7	167.1	
07_1P	-5.9	356.1	37.3	9.54E-04	1.4	61.3	-155.8	
05_9P	-7.1	342.5	57.7	4.15E-04	1.4	73.3	-108.3	Transition
05_6P	-7.4	369.1	30.4	4.48E-04	1.1	56.1	-179.3	
04_2P	-8.8	338.7	2.1	1.01E-03	3.8	38.3	-135.9	
03_8P	-9.2	308.2	-8.4	7.45E-04	2.3	-20.2	73.2	
03_0P	-10	327.2	-32.7	1.26E-03	0.7	-16.8	49.1	
01_5P	-11.5	339.3	-15.8	6.87E-04	5.3	-29.8	40.3	
01_2P	-11.8	338.1	3.7	6.12E-04	2.6	38.9	-134.8	
00_2P	-12.8	345.3	-38.7	7.03E-04	1.3	-17.6	30.9	
01_0M	-13.6	369.6	-6.3	8.70E-04	1.4	-36.8	4.5	Matuyama
01_2M	-13.8	371.8	-21.3	5.04E-04	3.8	-28.7	3.3	
01_8M	-14.4	315.8	-49.2	1.55E-03	1.2	-1.3	53.7	
02_7M	-15.3	320.5	-22.8	8.30E-04	4.2	-19.6	57.9	
03_5M	-16.1	341.7	-33.3	5.45E-04	0.6	-20.5	35.1	
04_2M	-16.8	305.2	-40.3	7.78E-04	1.1	-2.8	65.4	
05_6M	-18.2	305.9	-32.6	5.18E-04	1.2	-7.6	67.7	
05_8M	-18.4	362.3	-61	1.06E-03	1	-1.5	-165.2	
06_6M	-19.2	282.8	-65.3	3.19E-04	3.5	-27.5	-165.4	
08_0M	-20.6	320.1	-40.3	1.25E-04	5.4	-9.4	53.3	

08_2M	-20.8	335.3	-31.6	1.37E-03	0.3	-20	41.7
09_1M	-21.7	357.1	-58.1	1.40E-04	4.2	-1.8	18.8
10_0M	-22.6	352.5	-66.2	1.27E-03	1.5	-8.2	-158.4
10_5M	-23.1	393.7	-88.7	1.72E-03	1.4	-47.2	-165.6
12_7M	-25.3	102.8	-83.7	8.05E-04	3	-50.6	177.2
12_8M	-25.4	230.5	-72.3	8.44E-04	1.6	-59.6	-108.3
13_0M	-25.6	299.2	-56.6	1.04E-03	0.5	-11.9	-118.2
14.5M	-27.1	238	-68.7	9.90E-04	0.9	-54.2	-100.5
15_M	-27.6	312	-40.3	7.71E-04	2.5	-6	60
15_4M	-28	180.1	-89.3	8.56E-04	0.4	-50.8	-163.4
17_0M	-29.6	234.5	-79.1	9.03E-04	0.5	-57.6	-130.3
17_2M	-29.8	294.7	-60.7	2.11E-03	0.5	-16.9	-117.6
17_9M	-30.5	316.8	-82.8	1.56E-03	0.7	-38.3	-151.1
19_2M	-31.8	291.6	-87.8	4.43E-04	1.3	-47.5	-157.1
20_1M	-32.7	256.8	-72	1.24E-03	1.5	-45.9	-113.8
21_5M	-34.1	323.3	-23.4	3.91E-04	3.2	-20.5	55.1
22_0M	-34.6	250.8	-61.9	2.40E-03	0.3	-42.5	-94.3
22_5M	-35.1	143.3	-78.8	1.58E-03	0.4	-63.9	166.6

Fig. 4. Changes of magnetization directions on the Zijderveld diagram and Wulf stereonet during alternative field (AF) demagnetization method and demagnetization curve for typical samples (see Supporting Information Figs S2 for all other samples); (a) normal polarity from Brunhes section (12_0P, 13_0P) and (b) reversed polarity from Matuyama section (08_0M, 21_5M).

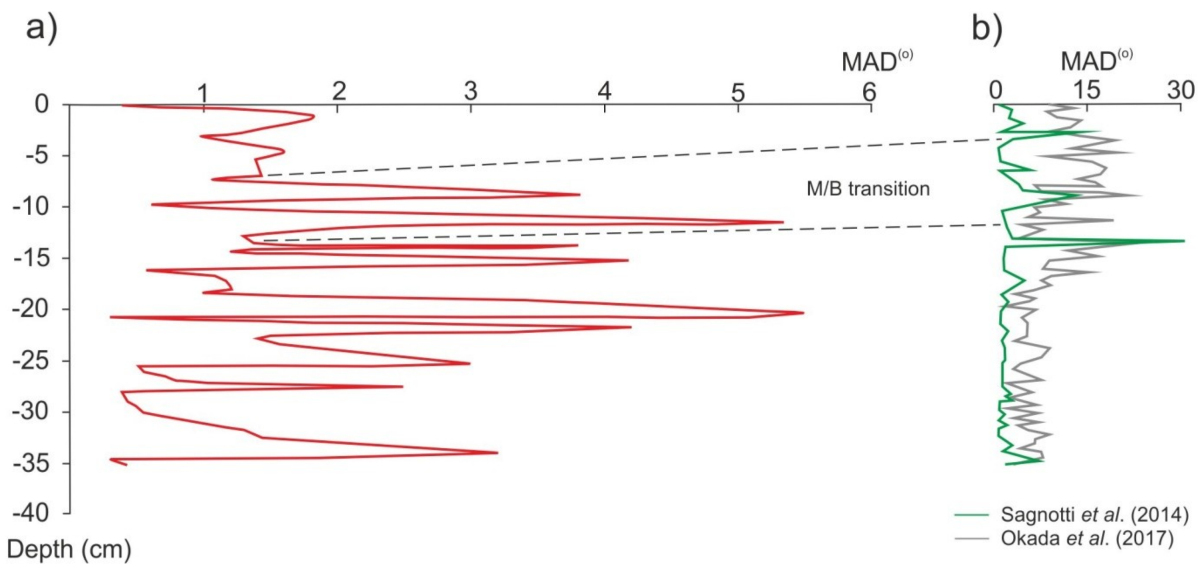

Fig. 5. Maximum angular deviation (MAD) changes during the Matuyama-Brunhes magnetic reversal a) from this data, b) from other published studies. Dashed lines show the M/B transition.

2.3. Rock Magnetism Measurements

To determine the magnetic minerals in the samples, High Temperature Magnetic Susceptibility measurements were done up to 635 °C by using an Agico Kappabridge MFK1-FA susceptibility meter. Samples used for the measurements are ZH01, ZH05, ZH30, ZH35 which correspond to the paleomagnetic samples 13_0P, 7_7P, 17_2M, 22_0M respectively. The samples for the susceptibility measurements ((χ) mass normalized) were chosen as a result of the paleomagnetic data.

3. Results

3.1. Paleomagnetic Results

The samples were demagnetized generally up to 20 mT (for details see Supporting Information Figs S2) which removed the viscous remanent magnetization (VRM) component causing a change in the direction of remanent magnetization during such demagnetization for most of the samples. This soft VRM component in the samples has a mean D: 13.8° and I: 56.8° values which is close to the present day's Earth's magnetic field direction values for the Czech Republic (D: 4.4° and I: 66.8°) (see Supporting Information Figs S3).

The intensity of the natural remanent magnetization (NRM) of the samples varies between 8.5-34.1e-3 A/m. Median destructive field (MDF) values where samples lost half of its magnetization range between 5-8 mT for the samples. NRM intensity and MDF values of the samples are shown in Supporting Information Figs S3. The maximum angular deviation (MAD) values for Matuyama and Brunhes sections are between 0.3°-5.4° (Fig. 5a). These values for the transition section are between 0.7°-5.3° which is relatively reliable for the detection of the migration of the paleomagnetic vector from reversed to normal polarity (Fig. 5a). The trend of the MAD values increases across the transition which can also be seen in the other studies (Sagnotti et al., 2014; Okada et al., 2017) (Fig. 5b).

In this study, paleomagnetic data showed inclination values changing by approximately 90° when measuring the sediment from 12.8 to 7.1 cm depth (Fig. 6). This revealed the transition nature of the Matuyama-Brunhes magnetic reversal in Za Hajovnou cave. Below this depth, there is a Matuyama section which has inclination fluctuations between -6.3°-88.7° (Fig. 6). Inclination angle changes between 33°-65.9° for Brunhes section above transition (Fig. 6). Also, the transition from reversed to normal polarity can be seen in declination data with similar depth. It has more frequent oscillations which show ~180° change from reversed to normal polarity between 2.5-9.2 cm depth (Fig. 6b). Despite the fluctuations, the intensity values of ChRM which can depend on the concentration variation of magnetic carriers of every individual sample were decreasing for the Matuyama section from the bottom to the transition between 35.1-15 cm depth (Fig. 6). After the transition from reversed to normal polarity, these values kept increasing which can be seen in the Brunhes section between 7.1-0 cm depth (Fig. 6). Fig. 6 shows the data in comparison with other studies that consisted of various sediment types and locations around the world. The depth of the data sets was normalized considering the transition zone and differences of sedimentation rate for each study and is not given in Fig. 5, 6. Even though there are some differences in absolute values, comparisons of this data set with other studies showed that fluctuations and frequency of fluctuations in our data are consistent with other data sets and serves as a supporting argument for Matuyama-Brunhes magnetic reversal in Za Hajovnou cave (Fig. 6).

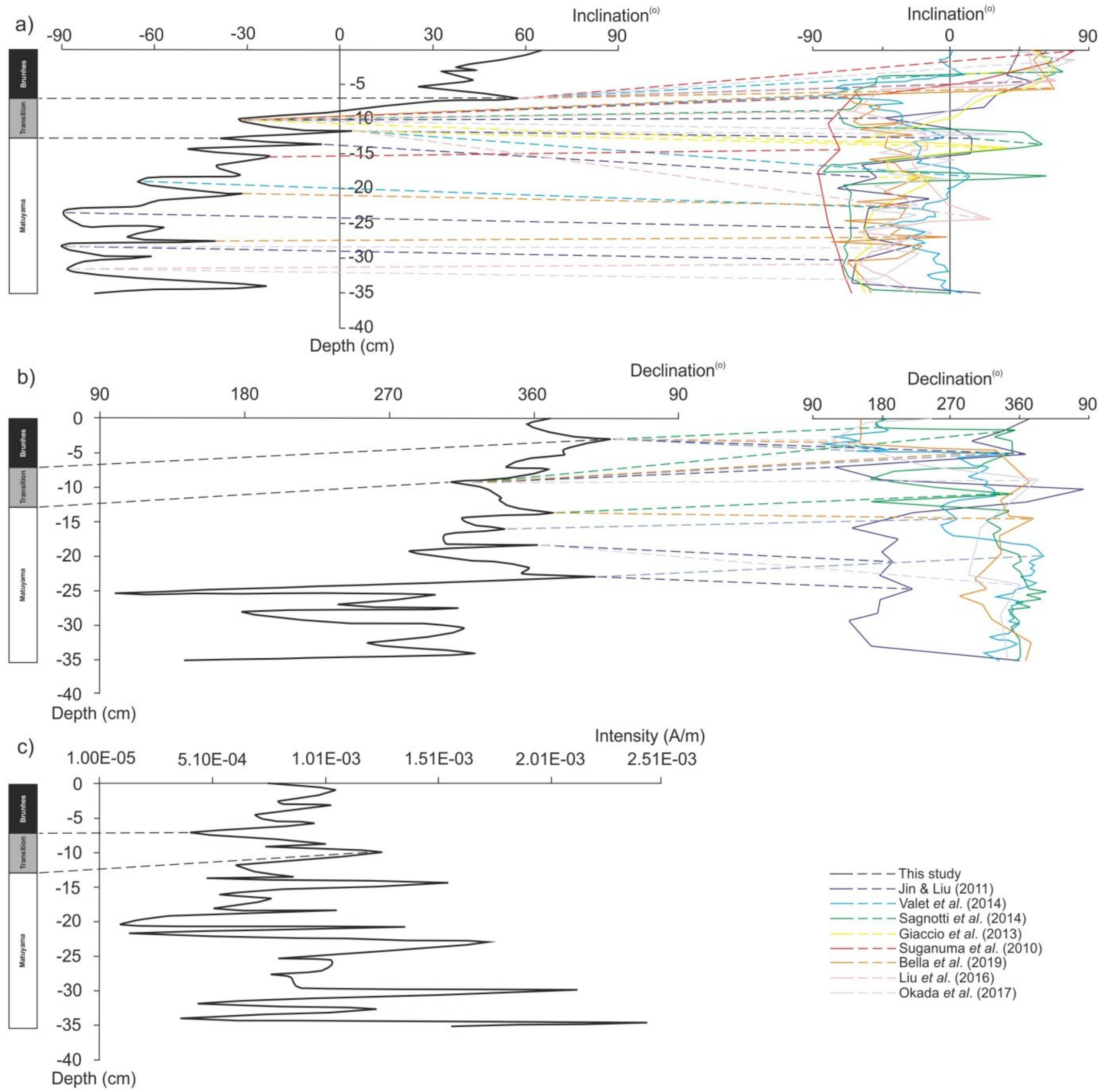

Fig. 6. Comparisons of inclination and declination data with previous studies. As a result of the alternative field demagnetization method, data shows (a) inclination, (b) declination, and (c) intensity of ChRM of the samples. Dashed lines in color connect sections of published studies and this study where we see the presentation of similar variation.

3.2. VGP's and Pole Migration

The virtual geomagnetic pole (VGP) shows the position of the geomagnetic paleopole (Lanza and Meloni, 2006). VGP's latitudes from this data set show fluctuations in the Matuyama section which are similar with the data from Yamazaki and Oda (2001) (Fig. 7a, b). These values indicate 90^{o} change from Matuyama to Brunhes transition as a result of pole migration (Fig. 7a). 75° change in VGP values at 11.8 cm depth (Fig. 7a) shows the precursor of the reversal according to Valet et al. (2012) (Fig. 7c). In addition, we plotted the VGP path for Matuyama, Brunhes, and transition sections using VGP latitudes and longitudes based on characteristic remanent magnetization (ChRM) directions detected in our samples (Fig. 8). VGP locations for the Matuyama section are in the southern hemisphere (Fig. 8). During the transition from reversed to normal polarity, the magnetic pole migrates from southern to northern hemisphere (Fig. 8). After the geomagnetic transition, paleopoles fluctuate around the geographic north pole (Fig. 8). This VGP path of pole migration during the transition from the southern to northern hemisphere compares well with the Matuyama-Brunhes transition found by Okada et al. (2017) recorded in marine sediments near Japan (Fig. 8).

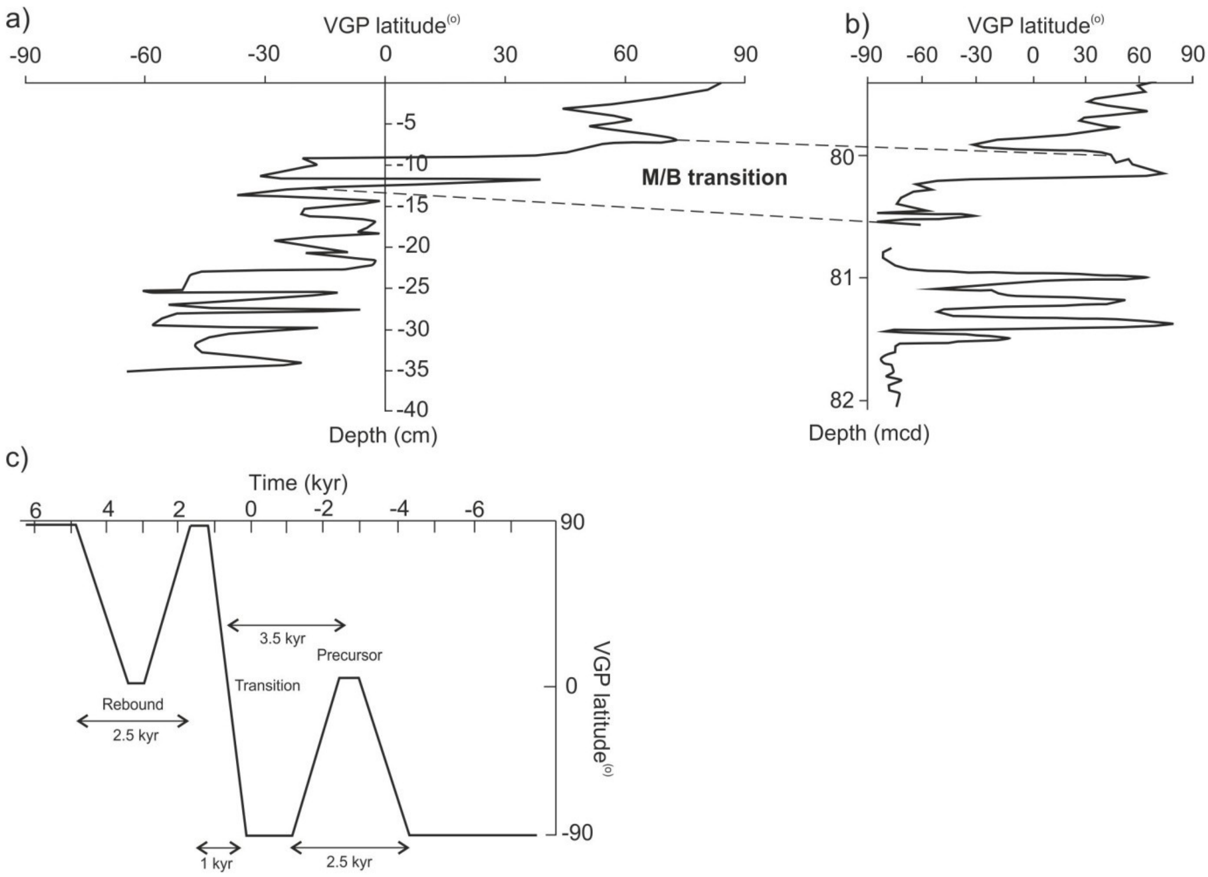

Fig. 7. Virtual geomagnetic pole (VGP) latitudes of a) this study, b) Yamazaki and Oda (2001), and c) shows the precursor model of Valet et al. (2012). Dashed lines show the main M/B transition for a) and b).

Fig. 8. Virtual geomagnetic pole (VGP) path of (a) this study and (b) VGP path of transition section from Okada et al. (2017) (dashed lines show similarities between two study).

3.3. Rock Magnetism Results

According to the High Temperature Magnetic Susceptibility measurements, the transition of maghemite to magnetite can be seen with an increase in susceptibility values at approximately 250-350 °C (Fig. 9). The samples have a Curie temperature between 530-550 °C which may be a sign of titanium in the minerals and of a new sulphite phase created from decomposing the maghemite and incorporation of the sulfur from the surrounding clay. The increase of susceptibility values in the cooling curves corresponds to the percentage of maghemite decrease after the heating in the samples (Fig. 9a, c, d). Two different drops in susceptibility values at 410 °C and 530 °C in Fig. 9c shows the existence of maghemite and magnetite together in the sample.

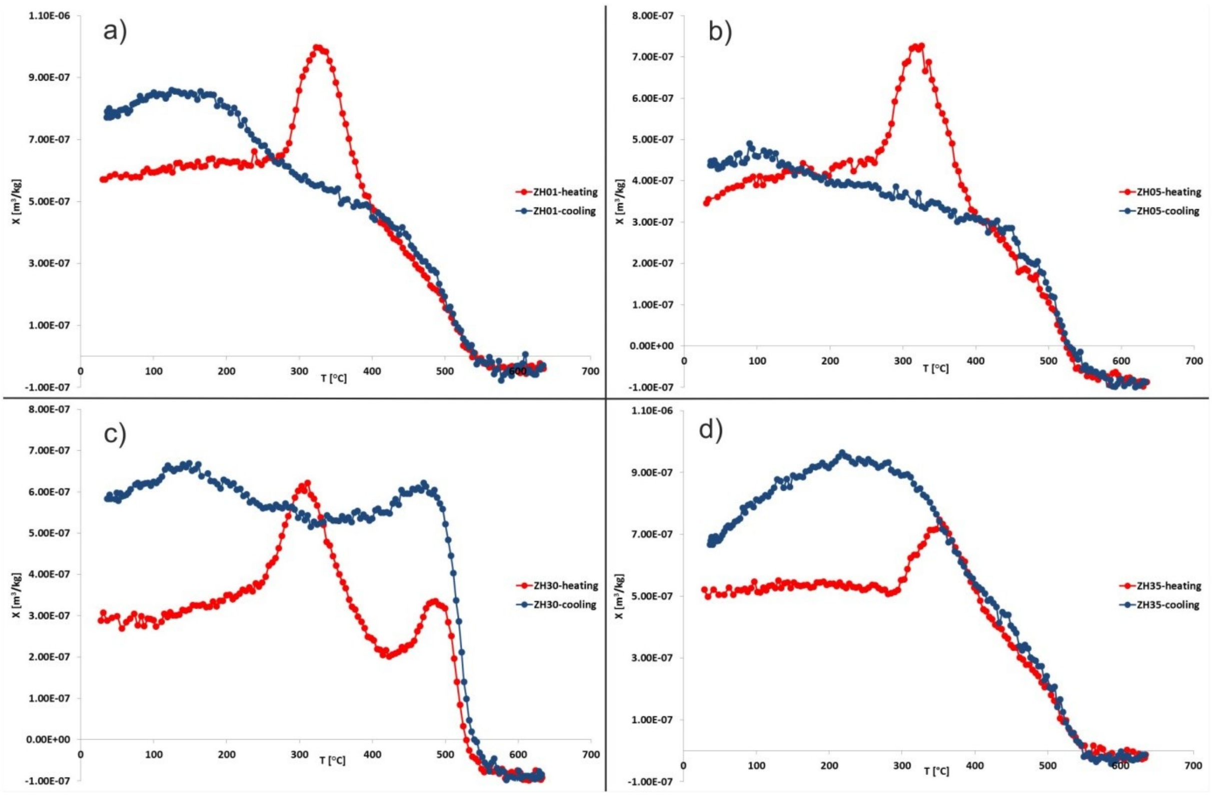

Fig. 9. High Temperature Magnetic Susceptibility measurement results (χ: mass normalized magnetic susceptibility, T: temperature in Celcius).

3.4. Sedimentation Rate Estimation

The sedimentation rate of the sediment from this study in the Za Hajovnou cave is not known. We compared the thickness of the transition section of our study (cm) with the thickness of the transition section of other studies (cm) and estimated the sedimentation rate. Let *n* be the ratio between the two data sets which shows how thick or thin the transition section of the previous study compared to our study (Equation 1.1, 1.2). This, we can estimate the sedimentation rate of Za Hajovnou (Equation 1.2). In equations, *tso* is the transition section thickness from our study (in cm), *tsp* is the transition section thickness of the published study (in cm), *srp* is the sedimentation rate of the published study (in cm/kyr), *sro* is sedimentation rate of our study (in cm/kyr).

Equations;

$$tso(cm)\,x\,n = tsp(cm)\,(1.1)$$

$$srp(cm/kyr)/n = sro(cm/kyr)\,(1.2)$$

Then, Za Hajovnou sedimentation rate ranges between 0.07-1.40 cm/kyr. Dropping the highest (1.41 cm/kyr) and lowest (0.066 cm/kyr) values gives rate between 0.2-1.0 cm/kyr. Thus, the average sedimentation rate is 0.6 cm/kyr. Sedimentation rate estimates compared with other studies are shown in Table 2.

Table 2. Sedimentation rate estimations for Za Hajovnou from the previous studies.

Reference	Sedimentation Rate	Sedimentation Rate*
Jin and Liu (2011)	15 cm/kyr	0.6 cm/kyr
Okada et al. (2017)	61 cm/kyr	0.91 cm/kyr
Sagnotti et al. (2010)	61 cm/kyr	0.6 cm/kyr
Giaccio et al. (2013)	26 cm/kyr	1 cm/kyr
Sagnotti et al. (2014)	21 cm/kyr	0.235 cm/kyr
Suganuma et al. (2010)	0.66 cm/kyr	0.23 cm/kyr
Bella et al. (2019)	0.64 cm/kyr	1.41 cm/kyr
Liu et al. (2016)	8.78 cm/kyr	0.066 cm/kyr

*: Sedimentation rate estimation for Za Hajovnou.

4. Discussion

Our data indicate that the Matuyama-Brunhes transition boundary constitutes 5.7 cm, between 7.1-12.8 cm depth of the sampled sedimentary section, of the Za Hajovnou cave sediment. The magnetic reversal is characterized and represented by frequent fluctuations of inclination angle (Fig. 6a) and VGP latitude (Fig. 7a). We think that oscillations in declination data show instability of the Earth's magnetic field. On the other hand, similar fluctuations which are seen in the previous studies (Fig. 6) show the reliability of the data.

Although the data in this study and Okada et al. (2017) belong to geographically different locations and sediment types, the similarity during polar migration (Fig. 8) shows that the reversal was a dipole transition, and the non-dipole field component was less significant (Oda et al., 2000; Mochizuki et al., 2011; Simon et al., 2019).

In most of the samples with demagnetization generally at 20 mT, some large fluctuations in the data may be considered as instability of remanent magnetization. Although some samples (01_8M, 04_2M, 17_2M, 17_9M, 22_0M) are not demagnetized up to 100 mT, it shows that minerals with low coercivity are responsible for the magnetization of the cave sediments in our study. It can be clearly seen in the rock magnetism measurements that the samples show similar behaviour during the measurements that is maghemite in this case.

Note that most of the section contains samples from the polarity transition. The data shows that the magnetic field was unstable for our oldest sample already, when in reversed polarity. This observation goes well with Yamazaki and Oda (2001) where they show the magnetic pole was unstable long time before the actual reversal boundary and the magnetic field started to fluctuate almost 150 cm deeper than the actual transition (Fig. 7b, 10). We think that our data illustrate the same instability, and this is why no paleomagnetic samples have VGP latitudes that deviate less than 25° from the reversed position. We provide a more detailed explanation of the reversed VGP behavior in our data that show reversed polarity unrest well before the actual magnetic reversal.

4.1. Precursor Event

Valet et al. (2012) showed a 90° change in VGP during reversed polarity before the transition from reversed to normal polarity (Fig. 7c). According to this model, the precursor prior to the magnetic reversal has a 2.5 kyr duration and it occurs ~ 3.5 kyr before the actual transition (mid-point) which has a 1 kyr duration (Fig. 7c). The model showed another 90° change as the rebound with 2.5 kyr duration after the transition (Fig. 7c). Sagnotti et al. (2014) reported Valet et al. (2012)'s precursor with 140° change in VGP, 0.7 kyr duration, and 5 kyr prior to the actual transition. In our VGP data (Fig. 7a), 75° change between 13.6-11.8 cm depth shows 3 kyr duration (according to 0.6 cm/kyr average sedimentation rate estimation) that can be interpreted as the precursor of the Matuyama-Brunhes magnetic reversal. The pick point of the precursor (11.8 cm depth) is 4.6 kyr before the actual transition (9.0 cm depth). The actual transition duration is 0.8 kyr between 9.2-8.8 cm. These values are consistent with the Valet et al. (2012) model and show the unique behaviour of the Earth's magnetic field during the reversal time. The rebound after the transition in the model is not seen in our study since VGP change between 7.1-3.2 cm is not enough to interpret it as the rebound.

4.2. Sediment Deposition and Sedimentation Rate

According to Lundberg et al. (2014) the cave was filled with water during the sedimentation which was continuously active without any climatic change or hiatus. This provides the continuous magnetic record of the reversal in the cave sediment and allows the sediment to acquire and keep the primary magnetization without the possibility of secondary mineralization. Also, there are no obvious marks in the studied sediment section that one would expect if breaks in deposition (e.g. lithological boundaries, desiccation cracks).

Our estimate of the Za Hajovnou cave's sedimentation rate (0.2 cm/kyr – 1.0 cm/kyr) seems to be significantly lower than the sediments from other studies (Sagnotti et al., 2010; Jin and Liu, 2011; Giaccio et al., 2013; Liu et al., 2016; Okada et al., 2017). This is likely due to contrasting sediment types. While the duration of the M/B transition was reported to last between 4-13 kyr (Yamazaki and Oda, 2001; Suganuma et al., 2010; Valet et al., 2014; Okada et al., 2017), the averaged sedimentation rate of 0.6 cm/kyr in this study suggests transition duration of 9.66 kyr (7.1-12.8 cm sediment transition depth section) and thus strengthen our confidence to the reliability of our sedimentation rate and paleomagnetic record estimates. Additionally, low sedimentation rates (<1 cm/kyr) were reported in previous Matuyama-Brunhes magnetic reversal studies (Clark, 1970; Love and Mazaud, 1997; Nowaczyk et al., 2001).

Analyzes of cave sediments by paleomagnetism carried out in different locations around the earth such as in Western Europe (Parés et al., 2018), South Africa (Nami et al., 2016), South America (Jaqueto et al., 2016), North America (Stock et al., 2005), Southern Europe (Pruner et al., 2010), Eastern Asia (Morinaga et al., 1992) showed that cave sediments recorded magnetic reversals. Morinaga et al. (1992) suggested a low sedimentation rate for the Western Japan cave sediments 1.6 cm/kyr which shows a similar rate with our Central European cave sediment estimation. King and Channell (1991) suggested that large "lock-in" depths are associated with interparticle rigidity and strength, characteristic of clayey low accumulation rate sediments (<1 cm/kyr) which results in delays of magnetic acquisition. This shows that magnetic polarity reversal could have a large (25 kyr) apparent age offset between sediments with high and very low accumulation rates (King and Channell, 1991).

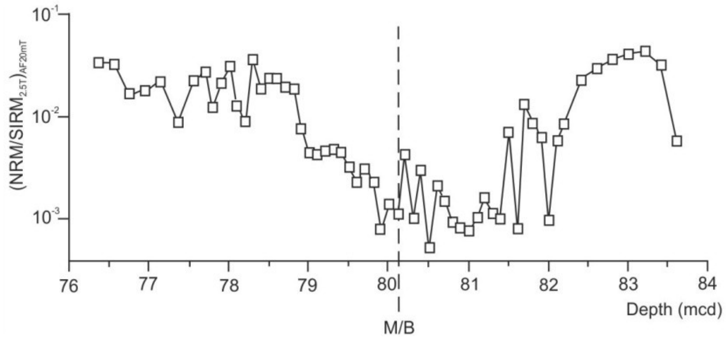

Fig. 10. NRM/SIRM ratio from Yamazaki and Oda (2001). The oscillations start from 81.6 mcd in the ratio below the reversal. Dashed lines shows the M/B reversal.

5. Conclusions

We compared the paleomagnetic data from the cave sediments with published magnetic reversal record and were able for the first time to use the detailed magnetic characteristic of cave sediment and to infer the specific magnetic reversal (Matuyama-Brunhes). This is possible due to the nature of the magnetic reversal that we discovered. Note that the paleopole was residing in the east of Africa and then quickly reappeared west of North America. We consider this as an important marker signature for dating the central European paleomagnetic record from this time period.

The precursor event in our data is a significant anomaly to identify the behaviour of the Matuyama-Brunhes magnetic reversal. Additionally, we were able to design a new method for estimation of the accumulation rate of the cave sediment in Za Hajovnou cave, which until now was not known.

Author contributions

HU and GK designed research and wrote the paper, JK contributed to the fieldwork, gave detailed information about the cave sediment, and commented significantly.

Acknowledgements

We thank Kristina Kdyrova for helping with sample preparation and measurements. Pruhonice Paleomagnetism Laboratory is thanked for allowing us to measure the cave sediment samples. Support for GK came from the Czech Science Foundation 20-08294S, 20-00892L, Ministry of Education, Youth and Sports LTAUSA 19141, and institutional support RVO 67985831.

This study is dedicated to our co-author Jaroslav Kadlec, who passed away recently.

References

Bábek, O., Briestenský, M., Přecechtělová, G., Štěpančíková, P., Hellstrom, J. C. and Drysdale, R. N., 2015. Pleistocene speleothem fracturing in the Western Carpathian orogenic foreland: A case study from transtensional setting at the eastern margin of the Bohemian Massif, *Geol. Q.,* **59**(3), 491-506, doi:10.7306/gq.1225.

Bella, P., Bosák, P., Braucher, R., Pruner, P., Hercman, H., Minár, J., Veselský, M., Holec, J. and Léanni, L., 2019. Multi-level Domica–Baradla cave system (Slovakia, Hungary): Middle Pliocene–Pleistocene evolution and implications for the denudation chronology of the Western Carpathians, *Geomorphology,* **327**, 62–79. doi:10.1016/j.geomorph.2018.10.002.

Bleil, U. and von Dobeneck, T., 1999. Geomagnetic Events and Relative Paleointensity Records — Clues to High-Resolution Paleomagnetic Chronostratigraphies of Late Quaternary Marine Sediments?, in *Use of Proxies in Paleoceanography*, 635-654, ed. Fischer, G. & Wefer, G., Springer, doi:10.1007/978-3-642-58646-0_26.

Butler, R. F., 1992. Paleomagnetism: magnetic domains to geologic terranes. *Paleomagn. Magn. domains to Geol. terranes,* Vol. 319, 56-57, Blackwell.

Channell, J. E. T., Hodell, D. A., Singer, B. S. and Xuan, C., 2010. Reconciling astrochronological and 40Ar/39Ar ages for the Matuyama-Brunhes boundary and late Matuyama Chron, *Geochem Geophy Geosy.,* **11**(12), 1–21, doi:10.1029/2010GC003203.

Clark, D. L., 1970. Magnetic reversals and sedimentation rates in the Arctic Ocean, *Geol. Soc. Am. Bull.,* **81**(10), 3129-3134, doi:10.1130/00167606(1970)81[3129:MRASRI]2.0.CO;2.

Giaccio, B., Castorina, F., Nomade, S., Scardia, G., Voltaggio, M. and Sagnotti, L., 2013. Revised Chronology of the Sulmona Lacustrine Succession, Central Italy, *J. Quat. Sci.,* **28**(6), 545–551, doi:10.1002/jqs.2647.

Gradstein, F. M., Ogg, J. G., Smith, A. G., Bleeker, W. and Lourens, L. J., 2004. A new Geologic Time Scale, with special reference to Precambrian and Neogene, *Episodes,* **27**(2), 83–100, doi:10.18814/epiiugs/2004/v27i2/002.

Gubbins, D. and Herrero-Bervera, E., 2007. *Encyclopedia of Geomagnetism and Paleomagnetism*, 588-589, Springer, doi:10.1007/978-1-4020-4423-6.

Haneda, Y., Okada, M., Suganuma, Y. and Kitamura, T., 2020. A full sequence of the Matuyama–Brunhes geomagnetic reversal in the Chiba composite section, Central Japan, *Prog. Earth Planet. Sci.*, **7**(1), 1-22, doi:10.1186/s40645-020-00354-y.

Jaqueto, P., Trindade, R. I. F., Hartmann, G. A., Novello, V. F., Cruz, F. W., Karmann, I., Strauss, B.E. and Feinberg, J.M., 2016. Linking speleothem and soil magnetism in the Pau d'Alho cave (central South America), *J. Geophys. Res. Solid Earth*., **121**(10), 7024-7039, doi:10.1002/2016JB013541.

Jin, C. and Liu, Q., 2011. Revisiting the stratigraphic position of the Matuyama-Brunhes geomagnetic polarity boundary in Chinese loess, *Palaeogeogr. Palaeoclimatol. Palaeoecol.,* **299**(1), 309–317, doi:10.1016/j.palaeo.2010.11.011.

Kadlec, J., Chadima, M., Pruner, P. and Schnabl, P., 2005. Paleomagnetic dating of sediments in the "Za Hájovnou" cave in Javoříčko, Natur. Stu. Museum Prostějov Reg., **8**, 75-82.

Kadlec, J., Čížková, K., and Šlechta, S., 2014. New updated results of paleomagnetic dating of cave deposits exposed in Za Hájovnou Cave, Javoříčko Karst *Acta Musei Natl. Pragae, Ser. B - Hist. Nat.,* **70**, 27-34, doi:10.14446/AMNP.2014.27.

King, J. W. and Channell, J. E. T., 1991. Sedimentary Magnetism, Environmental Magnetism, and Magnetostratigraphy, *Rev. Geophys.,* **29**, 358-370, doi:10.1002/rog.1991.29.s1.358.

Kirschvink, J. L., 1980. The least−squares line and plane and the analysis of palaeomagnetic data, *Geophys. J. R. Astron. Soc.,* **62**(3), 699-718, doi:10.1111/j.1365-246X.1980.tb02601.x.

Kitaba, I., Hyodo, M., Katoh, S., Dettman, D. L. and Sato, H., 2013. Midlatitude cooling caused by geomagnetic field minimum during polarity reversal, *Proc. Natl. Acad. Sci.,* **110**(4), 1215–1220, doi:10.1073/pnas.1213389110.

Lanza, R. and Meloni, A., 2006. *The earth's magnetism: An introduction for geologists*, 137-157, Springer, doi:10.1007/978-3-540-27980-8.

Liu, J., Liu, Q., Zhang, X., Liu, J., Wu, Z., Mei, X., Shi, X. and Zhao, Q., 2016. Magnetostratigraphy of a long Quaternary sediment core in the South Yellow Sea, *Quat. Sci. Rev.,* **144**, 1–15, doi:10.1016/j.quascirev.2016.05.025.

Love, J. J. Mazaud, A., 1997. A database for the Matuyama-Brunhes magnetic reversal, *Phys Earth Planet In*., **103**(3), 207-245, doi: 10.1016/S0031-9201(97)00034-4.

Lundberg, J., Musil, R. and Sabol, M., 2014. Sedimentary history of Za Hájovnou Cave (Moravia, Cze&ch Republic): A unique Middle Pleistocene palaeontological site, *Quat. Int.,* **339**, 11-24, doi:10.1016/j.quaint.2013.04.006.

Mochizuki, N., Oda, H., Ishizuka, O., Yamazaki, T. and Tsunakawa, H., 2011. Paleointensity variation across the Matuyama-Brunhes polarity transition: Observations from lavas at Punaruu Valley, Tahiti, *J. Geophys. Res. Solid Earth*, **116**(B6), doi:10.1029/2010JB008093.

Morinaga, H., Yaskawa, K. and Horie, I., 1992. A geomagnetic reversal recorded in a stalagmite collected in western japan, *J. Geomagn. Geoelectr.,* **44**(8), 661-675, doi:10.5636/jgg.44.661.

Muller, H., 1992. Climate Changes During and at the end of the Interglacials of the Cromerian Complex, in *Start of a Glacial,* 51-69, ed. Kukla, G.J. & Went, E., Springer. doi:10.1007/978-3-642-76954-2_5.

Musil, R., 2005. Jeskyně Za Hájovnou, vyjímečná lokalita Javořícského krasu, *Acta Musei Natl. Pragae, Ser. B - Hist. Nat*., **8**, 11-39.

Musil, R., 2014. The unique record of Za Hájovnou Cave, *Acta Musei Natl. Pragae, Ser. B - Hist. Nat.,* **70**, 7-26. doi:10.14446/AMNP.2014.7.

Musil, R., Sabol, M., Ivanov, M. and Doláková, N., 2014. Middle pleistocene stratigraphy of the deposits in Za Hájovnou Cave (Javořjčko Karst, Northern Moravia, Czech Republic), *Acta Musei Natl. Pragae, Ser. B - Hist. Nat.,* **70**, 107-119, doi:10.14446/AMNP.2014.107.

Nami, H. G., De La Peña, P., Vásquez, C. A., Feathers, J. and Wurz, S., 2016. Palaeomagnetic results and new dates of sedimentary deposits from Klasies River Cave 1, South Africa, *S. Afr. J. Sci.,* **112**(11), doi:10.17159/sajs.2016/20160051.

Nowaczyk, N. R., Frederichs, T. W., Kassens, H., Nørgaard−Pedersen, N., Spielhagen, R. F., Stein, R. and Weiel, D., 2001. Sedimentation rates in the Makarov Basin, central Arctic Ocean: A paleomagnetic and rock magnetic approach, *Paleoceanography*, **16**(4), 368-389, doi:10.1029/2000PA000521.

Oda, H., Shibuya, H. and Hsu, V., 2000. Palaeomagnetic records of the Brunhes/Matuyama polarity transition from ODP Leg 124 (Celebes and Sulu seas), *Geophys. J. Int.,* **142**(2), 319–338, doi:10.1046/j.1365-246X.2000.00130.x.

Okada, M., Suganuma, Y., Haneda, Y. and Kazaoka, O., 2017. Paleomagnetic direction and paleointensity variations during the Matuyama-Brunhes polarity transition from a marine succession in the Chiba composite section of the Boso Peninsula, central Japan 1, Geomagnetism. *Earth, Planets Sp.,* **69**, 1–19, doi:10.1186/s40623-017-0627-1.

Parés, J. M., Álvarez, C., Sier, M., Moreno, D., Duval, M., Woodhead, J. D., Ortega, A.I., Campaña, I., Rosell, J., de Castro, J.B. and Carbonell, E., 2018. Chronology of the cave interior sediments at Gran Dolina archaeological site, Atapuerca (Spain), *Quat. Sci. Rev.,* **186**, 1–16, doi:10.1016/j.quascirev.2018.02.004.

Parés, J. M., Arnold, L., Duval, M., Demuro, M., Pérez-González, A., Bermúdez de Castro, J. M., Carbonell, E. and Arsuaga, J.L., 2013. Reassessing the age of Atapuerca-TD6 (Spain): New paleomagnetic results, *J. Archaeol. Sci.,* **40**(12), 4586–4595, doi:10.1016/j.jas.2013.06.013.

Pol, K., Masson-Delmotte, V., Johnsen, S., Bigler, M., Cattani, O., Durand, G., Falourd, S., Jouzel, J., Minster, B., Parrenin, F. and Ritz, C., 2019. New MIS 19 EPICA Dome C high resolution deuterium data: Hints for a problematic preservation of climate variability at sub-millennial scale in the "oldest ice", *Earth Planet. Sci. Lett.,* **298**(1), 95-103, doi:10.1016/j.epsl.2010.07.030.

Pruner, P., Hajna, N. Z., Mihevc, A., Bosák, P., Man, O., Schnabl, P. and Venhodová, D., 2010. Magnetostratigraphy and fold tests from Račiška pečina and pečina v Borštu caves (classical karst, Slovenia), *Stud. Geophys. Geod.,* **54**, 27–48, doi:10.1007/s11200-010-0002-1.

Sagnotti, L., Budillon, F., Dinarès-Turell, J., Iorio, M. and MacRì, P., 2005. Evidence for a variable paleomagnetic lock-in depth in the Holocene sequence from the Salerno Gulf (Italy): Implications for "high- resolution" paleomagnetic dating, *Geochemistry, Geophys. Geosystems*., **6**(11), doi:10.1029/2005GC001043.

Sagnotti, L., Cascella, A., Ciaranfi, N., Macrì, P., Maiorano, P., Marino, M., and Taddeucci, J., 2010. Rock magnetism and palaeomagnetism of the montalbano jonico section (Italy):

Evidence for late diagenetic growth of greigite and implications for magnetostratigraphy, *Geophys. J. Int.,* **180**(3), 1049–1066, doi:10.1111/j.1365-246X.2009.04480.x.

Sagnotti, L., Scardia, G., Giaccio, B., Liddicoat, J. C., Nomade, S., Renne, P. R., and Sprain, C.J., 2014. Extremely rapid directional change during Matuyama-Brunhes geomagnetic polarity reversal, *Geophys. J. Int.,* **199**(2), 1110–1124, doi:10.1093/gji/ggu287.

Simon, Q., Suganuma, Y., Okada, M. and Haneda, Y., 2019. High-resolution 10Be and paleomagnetic recording of the last polarity reversal in the Chiba composite section: Age and dynamics of the Matuyama–Brunhes transition, *Earth Planet. Sci. Lett.,* **519**, 92-100, doi:10.1016/j.epsl.2019.05.004.

Singer, B.S., Jicha, B.R., Mochizuki, N. and Coe, R.S., 2019. Synchronizing volcanic, sedimentary, and ice core records of Earth's last magnetic polarity reversal, *Science advances,* **5**(8), 1-11, doi:10.1126/sciadv.aaw4621.

Stock, G. M., Granger, D. E., Sasowsky, I. D., Anderson, R. S. and Finkel, R. C., 2005. Comparison of U-Th, paleomagnetism, and cosmogenic burial methods for dating caves: Implications for landscape evolution studies, *Earth Planet. Sci. Lett.,* **236**(1), 388–403, doi:10.1016/j.epsl.2005.04.024.

Suganuma, Y., Yokoyama, Y., Yamazaki, T., Kawamura, K., Horng, C. S. and Matsuzaki, H., 2010. 10Be evidence for delayed acquisition of remanent magnetization in marine sediments: Implication for a new age for the Matuyama-Brunhes boundary, *Earth Planet. Sci. Lett.,* **296**(3), 443–450, doi:10.1016/j.epsl.2010.05.031.

Suganuma, Y., Okada, M., Horie, K., Kaiden, H., Takehara, M., Senda, R., Kimura, J.I., Kawamura, K., Haneda, Y., Kazaoka, O. and Head, M.J., 2015. Age of Matuyama-Brunhes boundary constrained by U-Pb zircon dating of a widespread tephra, *Geology*, **43**(6), 491-494, doi:10.1130/G36625.1.

Valet, J.P., Fournier, A., Courtillot, V. and Herrero-Bervera, E., 2012. Dynamical similarity of geomagnetic field reversals, *Nature*, **490**, 89-93, doi:10.1038/nature11491.

Valet, J. P., Bassinot, F., Bouilloux, A., Bourlès, D., Nomade, S., Guillou, V., Lopes, F., Thouveny, N. and Dewilde, F., 2014. Geomagnetic, cosmogenic and climatic changes across the last geomagnetic reversal from Equatorial Indian Ocean sediments, *Earth Planet. Sci. Lett.,* **397**, 67–79, doi:10.1016/j.epsl.2014.03.053.

Valet, J.P., Bassinot, F., Simon, Q., Savranskaia, T., Thouveny, N., Bourlés, D.L. and Villedieu, A., 2019. Constraining the age of the last geomagnetic reversal from geochemical and magnetic analyses of Atlantic, Indian, and Pacific Ocean sediments, *Earth Planet. Sci. Lett.*, **506**, 323-331, doi:10.1016/j.epsl.2018.11.012

Yamazaki, T. and Oda, H., 2001. A Brunhes-Matuyama polarity transition record from anoxic sediments in the South Atlantic (Ocean Drilling Program Hole 1082C), *Earth, Planets Sp.,* **53**(8), 817-827, doi:10.1186/BF03351679.

Žák, K., Lipták, V., Filippi, M., Orvošová, M., Hercman, H. and Matoušková, Š., 2018. Cryogenic carbonates and cryogenic speleothem damage in the za hájovnou cave (Javoříčko karst, Czech Republic), *Geol. Q.,* **62**(4), 829-839, doi:10.7306/gq.1441.

Zijderveld, J. D. A., 1967. Ac Demagnetization of Rocks: Analysis of Results, in *Methods in Palaeomagnetism,* 254-286, ed. Collinson, D.W., Elsevier.

Data Availability Statement

All data are incorporated into the article and its online supplementary material.

Supporting Information

Supplementary data are available online.

Supporting Information Tables S1: Demagnetization data for the samples.

Supporting Information Figures S2: Zijderveld diagrams, Wulf stereonets, and demagnetization curves of the rest of the samples for the alternative field (AF) demagnetization method.

Supporting Information Figures S3: NRM intensity, MDF values, and VRM data